Journal of Sustainable Built Environment

Research Article

https://doi.org/10.70731/199thc77

Factors Affecting the Seismic Performance of RBS Truss Chord Members under Combined Axial–Bending–Shear Loading

Yao Qu [a,b], **Tianhao Liu** [a,*], **Jiapeng Li** [b], **Ruoli Yang** [b], **Yue Chen** [c,d]

[a] *CUCDE Environmental Technology Co., Ltd., Beijing 100032, China*
[b] *Science and Technology and Industrialization Development Center, Ministry of Housing and Urban-Rural Development, Beijing 100835, China*
[c] *Beijing Advanced Innovation Center for Future Urban Design, Beijing 100044, China*
[d] *Beijing University of Civil Engineering and Architecture, Beijing 100044, China*

KEYWORDS

Super High-Rise Structure;
Outrigger Truss;
Reliability

ABSTRACT

In recent years, the outrigger truss has been widely used in super high-rise buildings. How to improve the seismic performance of the outrigger truss has become an important research front. It has been shown that the Reduced Beam Section (RBS) can perform local damage control and maximize the node guarantee. Connection performance, so in the super high-rise structure, Reduced Beam Section (RBS) truss chord can be used to improve the structural reliability, but the existing research on dog-bone joints is mostly the seismic performance of the bending-shear coupling node. There are few experimental studies on the seismic performance of dog-bone joints under compression-bending-shear coupling. In this paper, combined with the content of "structural reliability", considering the uncertainty of the structural resistance coefficient of steel structure, such as material properties, geometric parameters, calculation mode, etc., through the finite element simulation, the compression-bending-shear coupling of RBS truss chord The seismic performance under the action is studied, and the reliable index of the RBS chord string function function is solved. The research results of this paper provide reference for designers of super high-rise structures.

INTRODUCTION

With the rapid advancement of science and technology, high-rise buildings are springing up like bamboo shoots after a spring rain. According to statistics from the Council on Tall Buildings and Urban Habitat (CTBUH), the global distribution of super-tall buildings is shown in **Figure 1**. As of March 2019, there are 144 completed buildings worldwide that exceed 300 m in height, 69 of which are located in China—making it the country with the largest number of super-tall buildings in the world. The evolution of super-tall building structures encompasses the application of new materials, innovative structural systems, and advanced design concepts.

* Corresponding author. E-mail address: lthmelo@163.com

Received 12 August 2025; Received in revised from 25 August 2025; Accepted 15 September 2025; Published online 20 September 2025.

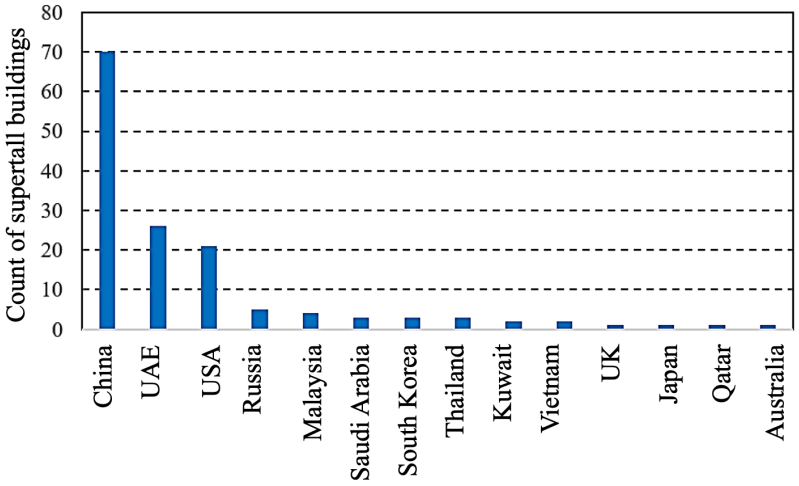

Figure 1 | Supertall-building counts by country

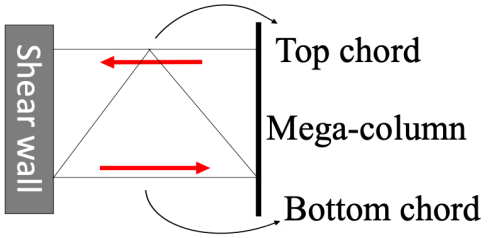

Figure 2 | Schematic force diagram of the outrigger truss

These developments not only address, to a significant extent, public concerns over efficient land use, but also constitute a vital component of the construction industry's future. Building upon the current characteristics of super-tall buildings, continuous innovation and optimization are essential to meet society's ever-growing demands—an issue that warrants our sustained attention.

Statistical data show that super-tall buildings erected since 2000 have widely adopted the hybrid lateral-force-resisting system of "mega-columns–core tube–outrigger"[1-3]. Among these components, the outrigger truss is the key element that links the mega-columns to the core tube, enabling them to resist lateral forces together and thereby enhancing the overall lateral stiffness. The outrigger truss is therefore one of the most critical members in the lateral-force-resisting system of such super-tall buildings.

The outrigger truss is a pivotal component in super-tall structures that connects the perimeter columns to the core. When the structure is subjected to horizontal loads, the core tube transforms the global bending moment into axial forces through the outrigger truss and transmits these forces to the perimeter columns. Consequently, the frame columns function like tension–compression members within the structural system, allowing the exterior frame and the core tube to share the lateral loads and improve the overall lateral resistance. A schematic representation of the forces in an outrigger truss is shown in **Figure 2**.

Continuous improvements in steel-manufacturing technology have raised the strength of structural steels and enhanced their overall performance, thereby promoting the wider use of steel structures in practical engineering. Prior to the 1990s, Q235 steel (then designated No. 3 steel) was extensively employed in structural applications; since the 1990s, Q345 steel has gradually become the predominant grade in building structures[4]. In recent years, the development of micro-alloying and thermo-mechanical controlled processing (TMCP) has led to the emergence of new high-strength structural steels[5].

Consequently, it is necessary to investigate these structural steels from a reliability perspective, establish appropriate design values, and ensure structural safety and reliability, thereby providing a scientific basis for refining relevant design codes. In this study, numerical simulations of the chord members with reduced beam section (RBS) in outrigger trusses are conducted and compared with existing experimental results to identify the reliability-sensitive controlling parameters for RBS outrigger trusses.

SPECIMEN DIMENSIONS AND LOADING PROTOCOL

The geometry of the reduced-beam-section (RBS) specimens is illustrated in **Figure 3**. Each test assembly consists of the specimen, gusset plates, and a base beam. The specimen is a welded H-section fabricated from Q345 structural steel; coupon tests determined the following material properties: yield strength f_y=364 MPa, tensile strength f_u=465 MPa, and elongation at fracture =43 %[6].

The specimen is welded to the gusset plates at the locations shown in Figure 3(d). The stiffness and strength of the gusset plates were verified, and flexural stiffeners were added to increase their bending rigidity. The gusset plates are bolted to the base beam.

Loading is displacement-controlled and follows a cyclic protocol. The widely used SAC loading protocol (Clark, 1997) is adopted: at drift ratios of 0.375%, 0.5%, and 0.75%, six cycles are applied at each level; beginning at a drift ratio of 1%, two cycles are applied at every subsequent level (1.5%, 2%, 3%, …). The loading history is depicted in **Figure 4**.

In the experimental program, the specimens were designed with axial compression ratios of μ^N=0.0

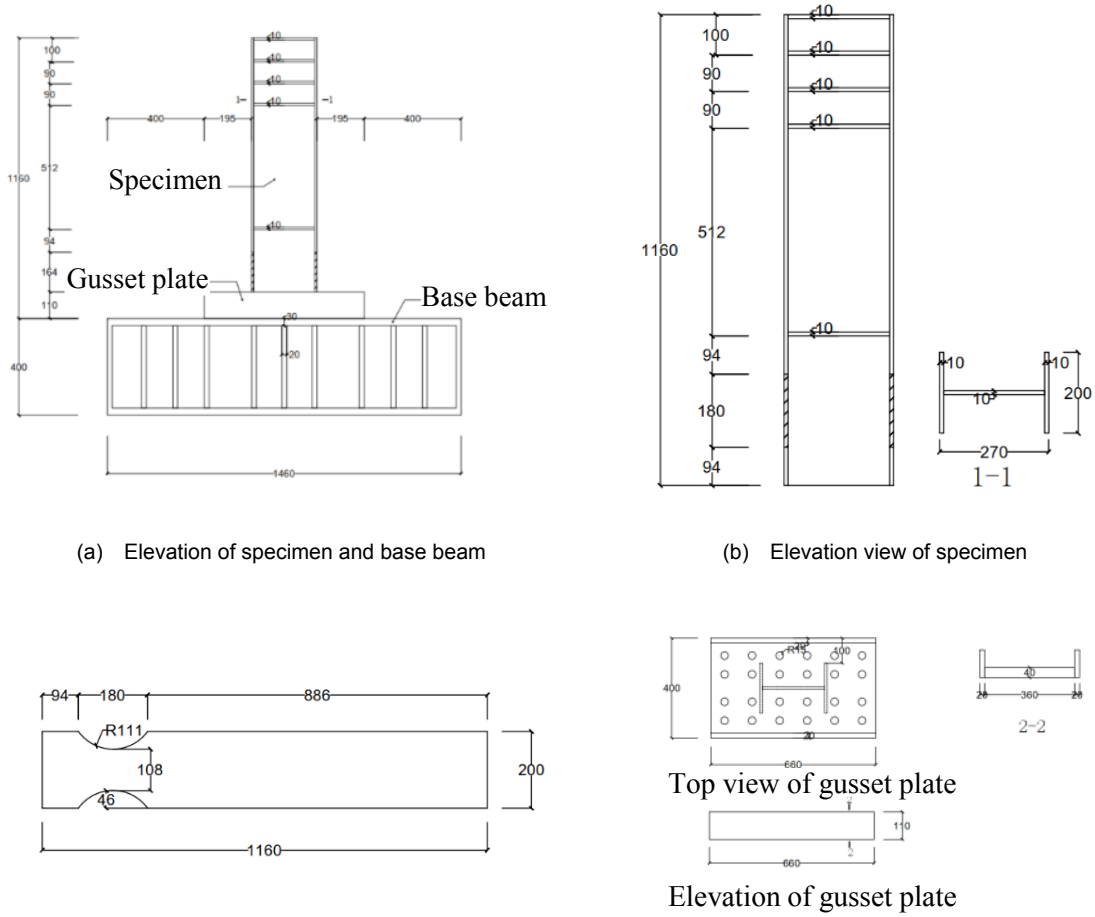

(a) Elevation of specimen and base beam

(b) Elevation view of specimen

(c) Top view of specimen

(d) Three orthographic views of gusset plate

Figure 3 | RBS specimen dimensions and details (unit: mm)

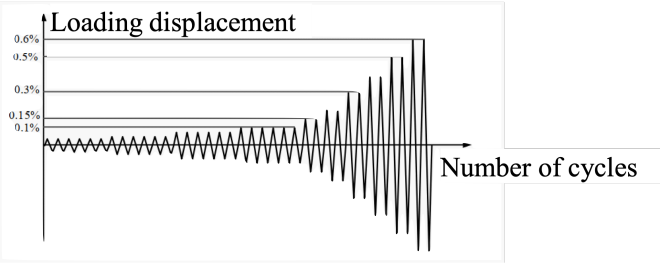

Figure 4 | Loading protocol

(specimen RBS00), μ^N=0.3 (specimen RBS03), and μ^N =0.5 (specimen RBS05). During loading, pushing was defined as positive displacement and pulling as negative displacement.

FINITE-ELEMENT SIMULATION

Building upon the beam-column joint tests conducted by Yang Qingshun at Tsinghua University and on previous domestic and international studies in this field, the general-purpose finite-element program MSC.Marc was employed to analyze representative specimens from the experimental program. Both material and geometric nonlinearities, the boundary conditions imposed during testing, and the effects of welded connections were incorporated in the establishment and solution of the finite-element models. Comparison between experimental and numerical results verified the accuracy and effectiveness of the finite-element model for predicting the behavior of chord joints with reduced-beam-section (RBS) outrigger trusses. Additional parametric analyses were then performed to identify the factors that influence the ultimate capacity of these joints, thereby facilitating the determination of key parameters that affect component reliability indices. The finite-element simulations compensate for the limitations of experimental studies in terms of specimen quantity and measurement constraints, provide a reliable basis for calculating the ultimate capacity of RBS outrigger-truss chord joints, and offer guidance for the development of design procedures for such components.

Introduction to the Finite-Element Software

MSC.Marc is a comprehensive, advanced nonlinear finite-element program with powerful structural analysis

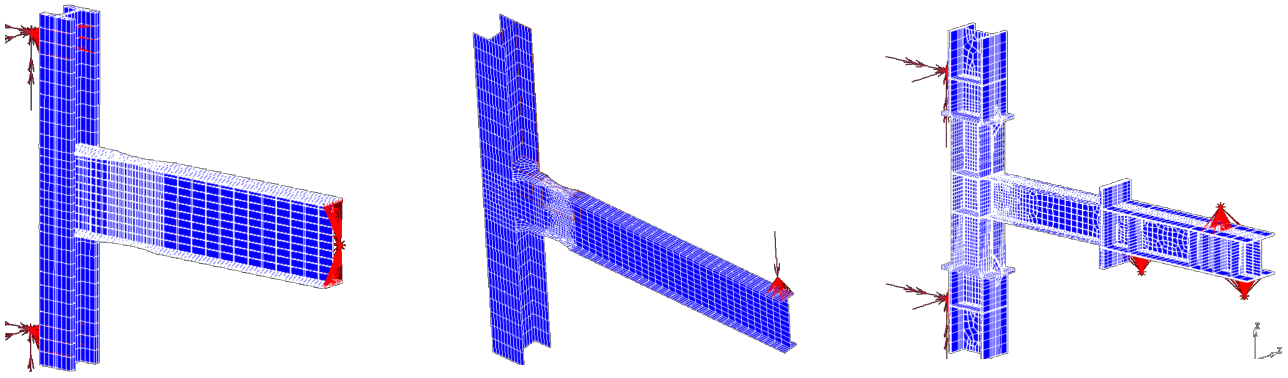

（a）cw-　　（b） cw-2　　（c）oj

Figure 5 l Finite-element model of RBS

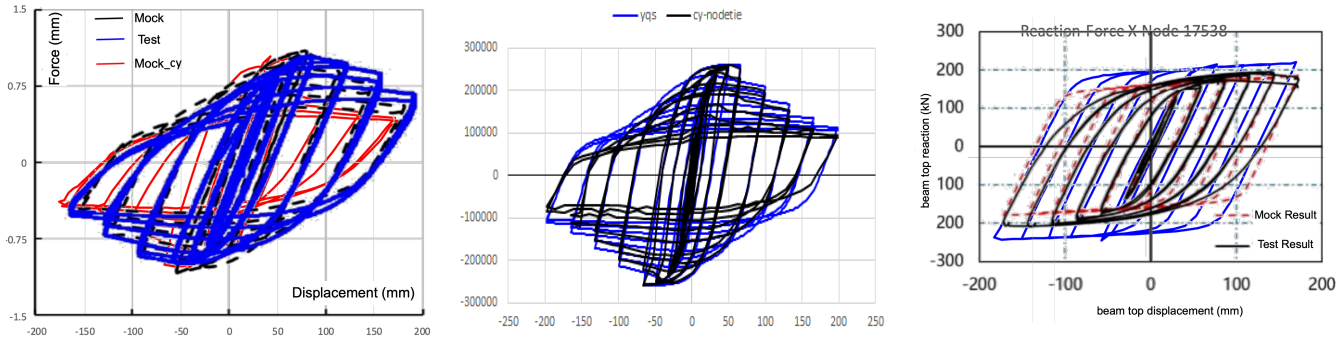

（a）cw-　　（b） cw-2　　（c）oj

Figure 6 l Validation of RBS FE model under bending–shear coupling

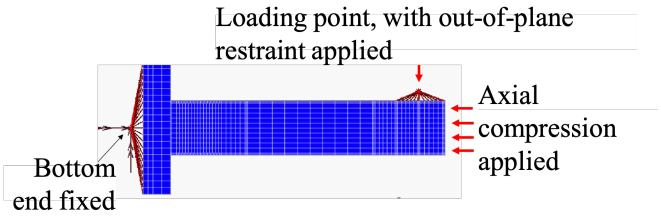

Figure 7 | Refined FE model of RBS outrigger-truss chord joint

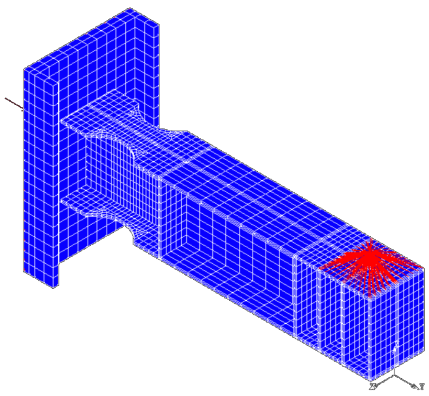

Figure 8 l Refined FE model of RBS outrigger-truss chord joint

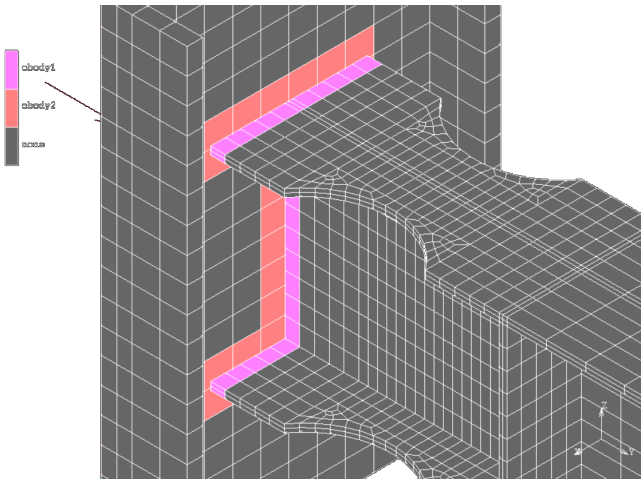

Figure 9 l Contact interactions in the refined FE model of RBS outrigger-truss chord joint

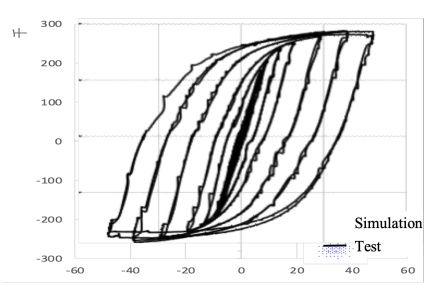

(a) Specimen RBS00 – Force–displacement hysteretic curve

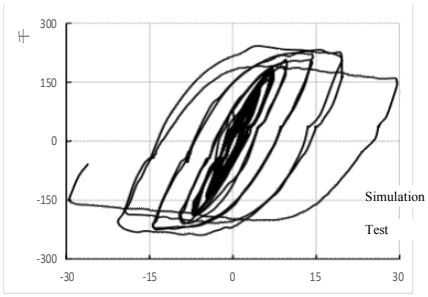

(b) Specimen RBS03 – Force–displacement hysteretic curve

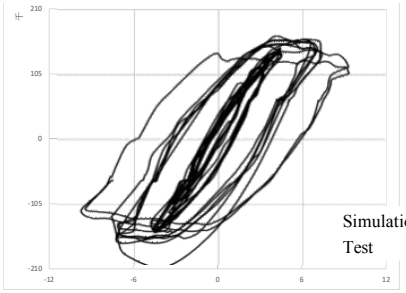

(c) Specimen RBS05 – Force–displacement hysteretic curve

Figure 10 | Comparison of hysteretic curves between experimental results and FE simulations (Unit: kN-mm)

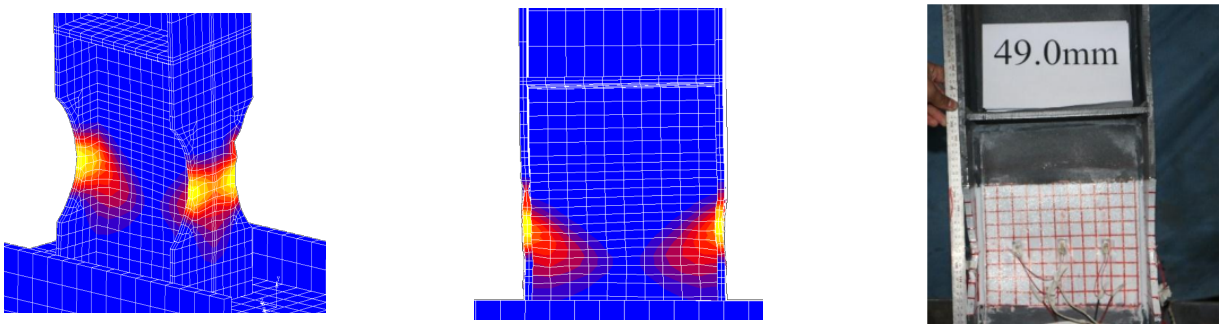

(a) Comparison of damage locations between FE model and test results for RBS00

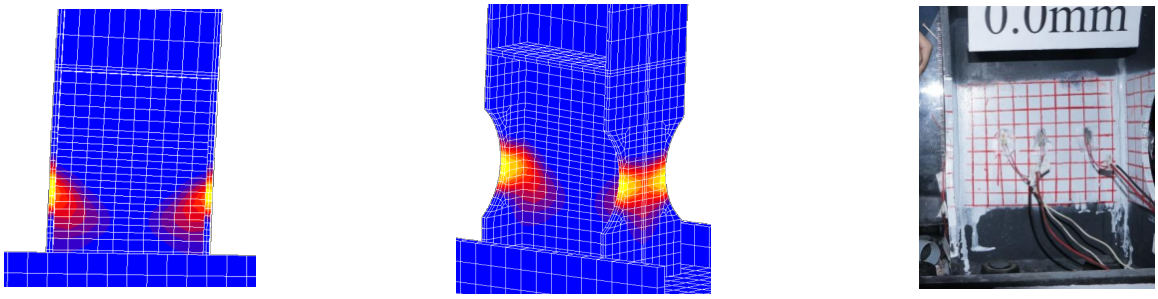

(b) Comparison of damage locations between FE model and test results for RBS03

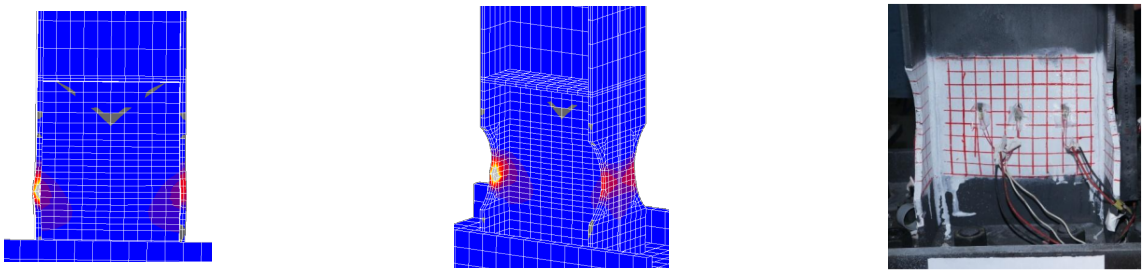

(c) Comparison of damage locations between FE model and test results for RBS05

Figure 11 | Comparison of damage locations between FE model and experimental results

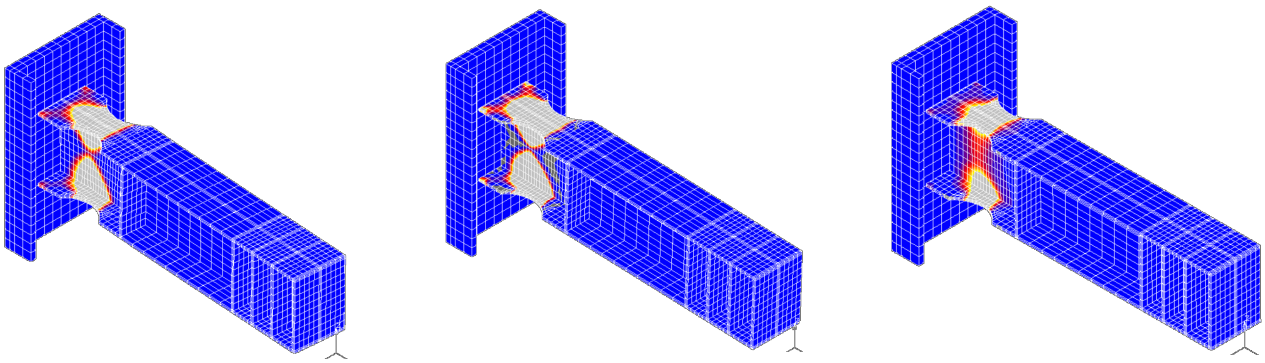

(a) Plastic zone in RBS00 FE model (b) Plastic zone in RBS03 FE model (c) Plastic zone in RBS05 FE model

Figure 12 | Plastic zones in RBS FE models

capabilities. It can address a wide range of linear and nonlinear problems, including linear/nonlinear static analysis, modal analysis, harmonic response analysis, spectrum analysis, random vibration analysis, dynamic response analysis, automatic static/dynamic contact, buckling/instability, and failure/damage analysis. All models presented in this chapter were developed and analyzed using MSC.Marc 2012.

Validation of the Finite-Element Model

To demonstrate that the developed FE model can reliably reproduce the mechanical behavior of RBS specimens under combined bending–shear loading, its accuracy was verified by simulating the tests reported by Uang[7] and Hu Yang-yang[8]. The finite-element mesh shown in **Figure 5** was established, and the simulated force–displacement hysteretic curves were compared with the experimental results. The comparison, presented in **Figure 6**, shows good agreement between the test data and the FE predictions. Consequently, the model can be adopted as a dependable baseline for investigating the rotational capacity of RBS sections subjected to combined axial–bending–shear loading.

Geometric Model

In constructing the finite-element models, every FE specimen was assigned the identical geometric dimensions measured in Yang Qingshun's tests. The boundary conditions imposed by the test setup were reproduced in detail: RBE2 *S-type links in MSC.Marc were introduced at the out-of-plane restraint cleats, at the hinged support at the specimen base, and at the actuator loading points, thereby precisely defining the constraints applied to the specimens. **Figure 7** and **Figure 8** illustrate the refined finite-element models of the RBS outrigger-truss chord joints.

Contact interactions were defined throughout the model. The interfaces between the loading stub and the test joint's column, the loading beam and the test joint's beam, and the underside of the test joint's beam flange and the upper flange of the column were all modeled with the Glue contact option in MSC.Marc, as illustrated in **Figure 9**. In Marc, surfaces linked by a Glue contact are enforced to be fully compatible, eliminating any relative displacement or separation between them.

Material Properties

Q345B structural steel is used throughout the model. The steel plates are represented by an ideal elastic–perfectly-plastic material law; no post-peak softening branch is considered. For all steel grades the elastic modulus is taken as 2.05×10^5 MPa. The von Mises yield criterion with associated flow rule is adopted, and a kinematic hardening law governs the plastic response. Both geometric nonlinearity and large deformation effects are activated so that local buckling of plates within the joint can be captured accurately.

Simulation Validation

Figure 10 compares the hysteretic curves obtained from the finite-element analyses with the experimental results of Yang Qingshun. The comparison shows that the numerical predictions are generally reliable for specimens with axial compression ratios (μ^N) of 0.0 and 0.3, whereas the yield strength deviates appreciably for μ^N 0.5.

More specifically:

For μ^N=0.0 and 0.3, the beam-end load–displacement curves predicted by the FE model closely match the test data.

For μ^N=0.5, the correlation deteriorates. Although the ultimate capacity predicted by the FE model differs from the test value by less than 10 %, the initial stiffness and post-yield stiffness agree reasonably well. The post-yield unloading stiffness observed in the test, however, is markedly lower than that predicted numerically.

Possible reasons for the discrepancy at μ^N=0.5 include: Slight differences between the actual material properties of the test specimen and those assigned in the FE model. Minor deviations in the boundary conditions and in the representation of the welds at the RBS outrigger-truss chord joint within the numerical model.

Figure 11 compares the damage patterns obtained from the finite-element analyses with the experimental observations. In all cases, local buckling initiates in the

Table 1 | Coefficient of variation

Steel	thickness group t / mm	Mean f_y / MPa	Standard deviation σ / MPa	Coefficient of variation δ
Grade 3 steel	4 ≤ t ≤ 20	280.7	22.6	0.081
	20 ≤ t ≤ 40	253.6	26.0	0.103
	40 ≤ t ≤ 60	234.9	21.7	0.092
16 Mn steel	t ≤ 16	383.2	24.8	0.065
	16 < t ≤ 25	355.7	23.5	0.066
	25 < t ≤ 38	348.2	29.1	0.084
	38 < t ≤ 50	343.6	31.3	0.091
Q235	t ≤ 16	301.9	28.6	0.095
	16 < t ≤ 40	304.5	44.2	0.145
Q345	t ≤ 16	388.7	28.0	0.073
	16 < t ≤ 35	371.8	29.1	0.078
	35 < t ≤ 50	363.3	28.2	0.078
	50 < t ≤ 100	371.6	35.3	0.095

Table 2 | Statistical parameters for geometric uncertainty [12]

Thickness range / mm	Mean value	Coefficient of variation
>6~16	0.980	0.050
>16-35	0.983	0.048
>35~50	0.986	0.045
>50~100	0.990	0.042

flanges and web of the reduced section of the RBS outrigger-truss chord joint. The numerically predicted damage states for the three axial-compression ratios are in good agreement with the experimental results reported by Yang Qingshun.

Figure 12 illustrates the plastic-zone distribution predicted by the finite-element analyses. The results demonstrate that introducing the reduced-beam-section (RBS) effectively confines the plasticity to the intended region of the outrigger-truss chord. Under the presence of axial force, the section yields earlier and buckles sooner, indicating that the RBS chord is highly sensitive to axial load. Designers should therefore pay particular attention to the influence of axial force on the performance of RBS outrigger-truss chords.

UNCERTAINTY ANALYSIS

Material Uncertainty

Material uncertainty captures the discrepancy between the actual mechanical properties of steel and their nominal values. This discrepancy stems from two sources: (i) the inherent variability of the material itself and (ii) the influence of standard test conditions on the measured properties. Extensive domestic surveys have been conducted in China to quantify these uncertainties for ordinary-strength structural steels. The statistical parameters obtained from these investigations are summarized in **Table 1**.

Material uncertainty arises from two distinct sources: (1) Test-related uncertainty, denoted as K_0, which accounts for variability introduced by the testing procedure itself; and (2) The inherent deviation between the actual material properties and the nominal (standard) values specified in product standards.Combining these two contributions yields the overall material-performance uncertainty factor K_M, expressed as

$$K_M = K_0 \times K_f \tag{1}$$

where K_f denotes the inherent variability of the material property itself, calculated by Equation (4-2):

$$K_f = f_y \div f_k \tag{2}$$

Where fy is the yield strength obtained from tests and f_k is the nominal yield-strength value specified in the relevant product standard. From this, the mean $\mu_{\mathrm{K_M}}$ and the coefficient of variation $\delta_{\mathrm{K_M}}$ of the overall material-performance uncertainty factor are expressed as:

$$\mu_{K_M} = \mu_{K_0} \times \mu_{K_f} \quad (3)$$

$$\delta_{\mathrm{K_M}} = \sqrt{\delta_{\mathrm{K_0}}{}^2 \cdot \delta_{\mathrm{K_f}}{}^2} \quad (4)$$

where $\mu_{\mathrm{K_0}}$ and $\delta_{\mathrm{K_0}}$ denote the mean and coefficient of variation of the test-related uncertainty K_0, while $\mu_{\mathrm{K_f}}$ and $\delta_{\mathrm{K_f}}$ are the mean and coefficient of variation of the inherent material-property uncertainty K_f.

Uncertainty in Geometric Parameters

Uncertainty in geometric parameters reflects the deviation between the measured and nominal values of quantities such as plate thickness, section height, width, cross-sectional area, moment of inertia, and member length.

The Central Research Institute of Building & Construction (MCC Group) collected extensive measured data from ten domestic steel fabricators, covering both plates and rolled sections. All measurements were classified according to the thickness categories stipulated in the relevant product standards. Statistical analysis revealed that negative rolling tolerances are prevalent in China's steel production; the thinner the plate, the more pronounced the negative deviation becomes. Consequently, the final statistical parameters are provided on a thickness-group basis in **Table 2**.

CONCLUSIONS

Comparative analyses of numerical simulations and experimental validation demonstrate that reduced-beam-section (RBS) outrigger-truss chords can successfully relocate plastic hinges and confine damage to predetermined locations. However, their mechanical response is highly sensitive to axial compression: the larger the axial compression ratio, the earlier the member yields. In addition, discrepancies between simulated and measured results are primarily attributable to uncertainties in material properties and geometric dimensions.

References

1. Lu, Xiao. Seismic Collapse and Performance Studies of Super-Tall Mega-Column–Core-Tube–Outrigger Structures [D]. Beijing: Tsinghua University, 2013.
2. Xie, Lin-lin. Performance-Based Design for Post-Earthquake Functional Recoverability of Mega-Column–Core-Tube–Outrigger Super-Tall Buildings under Strong Ground Motions [D]. Beijing: Tsinghua University, 2016.
3. Yang, Qing-shun. Experimental Investigation and Design Methods of Energy-Dissipating Outrigger Trusses [D]. Beijing: Tsinghua University, 2017.
4. Li, Guo-qiang; Wang, Yan-bo; Chen, Su-wen; et al. Research Status of High-Strength Structural Steels and Issues in Their Application in Seismic Regions. Journal of Building Structures, 2013, 34(1): 1-13.
5. Ban, Hui-yong; Shi, Gang; Shi, Yong-jiu; et al. Progress in Mechanical Properties of High-Strength Structural Steels for Buildings. Building Structures, 2013, 43(2): 88-94.
6. Yang, Qing-shun; Zhen, Wei; Xie, Lin-lin; Lu, Xin-zheng. Experimental Study on Seismic Performance of Energy-Dissipating Outrigger Trusses. Engineering Mechanics, 2016, 33(10): 76-83.
7. Gilton, Chad S.; Uang, Chia-Ming. Cyclic Response and Design Recommendations of Weak-Axis Reduced Beam Section Moment Connections. Journal of Structural Engineering, 2002, 128(4): 452-463.
8. Hu, Yang-yang; Lin, Xu-chuan; Wu, Kai-lai; Wang, Tao. Experimental Study on Seismic Behavior of Welded High-Strength Steel Beam–Column Joints with "Fuse" Gusset Plates. Engineering Mechanics, 2017, 34(Suppl.): 143-148.
9. Chen, Guo-xing; Li, Ji-hua. Statistical Parameters of Material Strength and Cross-Sectional Geometric Properties of Steel Members. Journal of Chongqing Institute of Architecture and Engineering, 1985, 7(1): 1-23.
10. Dai, Guo-xin; Li, Ji-hua; Xia, Zheng-zhong. Analysis and Research on Properties of Thick Steel Plates. Journal of Chongqing Institute of Architecture and Engineering, 1993, 15(2): 1-7.
11. Dai, Guo-xin; Li, Long-chun. Statistics and Analysis of Mechanical Properties of New Structural Steels for Buildings. Building Structures, 2000, 30(4): 31-32.
12. Central Research Institute of Building & Construction Co., Ltd., MCC; Revision Task Group for GB 50017-2003 Code for Design of Steel Structures. Experimental Investigation, Statistical Analysis and Design Values of Domestic Structural Steel for Buildings. Beijing: Central Research Institute of Building & Construction Co., Ltd., 2012.